Available online at www.sciencedirect.com
SCIENCE DIRECT®
Proceedings of the Combustion Institute 30 (2005) 447–453
Proceedings of the Combustion Institute
www.elsevier.com/locate/proci

Structure of partially premixed *n*-heptane–air counterflow flames

Paolo Berta[a], Ishwar K. Puri[b,*], Suresh K. Aggarwal[a]

[a] *Department of Mechanical and Industrial Engineering (M/C 251), University of Illinois at Chicago, 842 W. Taylor St., Chicago, IL 60607-7022, USA*
[b] *Department of Engineering Science and Mechanics, Virginia Polytechnic Institute and State University, 223 Norris Hall-MC 0219, Blacksburg, VA 24061, USA*

Abstract

To avoid the complexities associated with the droplet/vapor transport and nonuniform evaporation processes, a fundamental investigation of liquid fuel combustion in idealized configurations is very useful. An experimental–computational investigation of prevaporized *n*-heptane nonpremixed and partially premixed flames established in a counterflow burner is described. There is a general agreement between various facets of our nonpremixed flame measurements and the literature data. The partially premixed flames are characterized by a double flame structure. This becomes more distinct as the strain rate decreases and partial premixing increases, which also increases the separation distance between the two reaction zones. The peak partially premixed flame temperature increases with increasing premixing of the fuel stream. The peak CO_2 and H_2O concentrations are relatively insensitive to partial premixing. The CO and H_2 peak concentrations on the premixed side increase as the fuel-side equivalence ratio decreases. These species are transported to the nonpremixed reaction zone where they oxidize. The C_2 species have peaks in the premixed reaction zone. The concentrations of olefins are ten times larger than those of the corresponding paraffins. The oxidizer is present in partially premixed flames throughout the combustion system and there are no regions characterized by simultaneous high temperature and high fuel concentration. As a result, pyrolysis reactions leading to soot formation are greatly diminished.

Keywords: Partially premixed flame; Nonpremixed flame; Liquid fuel combustion; *n*-Heptane counterflow flame

1. Introduction

Liquid fuels are an important energy source, since they are used in numerous propulsion and energy conversion applications. The characteristics of liquid fuel combustion are very complex. The fuel is introduced into the combustion chamber in the form of a spray that consists of droplets with a wide size and velocity distribution, resulting in disparate vaporization rates. To avoid the complexities associated with the droplet/vapor transport and nonuniform evaporation processes, a fundamental investigation of liquid fuel combustion in idealized configurations is very useful. Such an investigation can also facilitate the validation of fundamental theoretical/computational models through measurements in flames. However, there is a paucity of such measurements in the literature [1,2]. We report on such an investigation. Although most practical liquid fuels are

* Corresponding author. Fax: +1 540 231 4574.
E-mail address: ikpuri@vt.edu (I.K. Puri).

1540-7489/$ - see front matter
doi:10.1016/j.proci.2004.08.141

blends of several components, we have examined *n*-heptane for its role as a surrogate liquid fuel for sake of simplicity. It is also a reference fuel in the definition of the octane number, and its oxidation chemistry has been extensively investigated.

Partially premixed flames contain a rich premixed fuel–air mixture in a pocket or stream, and, for complete combustion to occur, they require the transport of oxidizer from an appropriately oxidizer-rich (or fuel–lean) mixture that is present in another pocket or stream. Partial oxidation reactions occur in fuel-rich portions of the mixture, and any remaining unburned fuel and/or intermediate species are consumed in the oxidizer-rich portions. Partially premixed flames are important in numerous applications. They are relevant to turbulent nonpremixed combustion, which can contain regions where local extinction occurs, followed by partial premixing and re-ignition. Partially premixed combustion plays a fundamental role in the stabilization of lifted nonpremixed flames in which propagating premixed reaction zones anchor a nonpremixed reaction zone. In addition, droplet-containing group flames contain regions of partially premixed combustion. These flames are also important in most liquid-fueled combustion devices including gas turbine, diesel, and rocket engine combustors.

Due to their diverse applications and relevance, partially premixed flames have been investigated extensively in recent years. The bulk of the fundamental studies have focused on methane–air flames (e.g. [3,4]), motivated perhaps by the fact that detailed reaction mechanisms are available to model the chemistry. With the exception of a few recent investigations [1,5–8], the literature regarding the burning of higher hydrocarbon fuels, especially liquid fuels, in partially premixed flames is relatively sparse. In this investigation, we report on an experimental–computational investigation of *n*-heptane partially premixed flames established in a counterflow burner. Our objective is to provide detailed experimental data that can be subsequently used for the validation of computational models and reaction mechanisms involving simulations of liquid fuels in general, and *n*-heptane in particular.

2. Experimental apparatus

The separation distance between the nozzles of the counterflow burner was 15 mm and their diameter was 27.38 mm. The fuel was introduced from the bottom nozzle. A nitrogen curtain was established through an annular duct surrounding the fuel jet to isolate the flame from ambient disturbances. The nitrogen and burned gases were exhausted and cooled through another annular duct around the oxidizer nozzle. A detailed schematic diagram of the experimental setup is presented in Fig. 1. The velocities of the two streams were chosen to conform to the global strain rate [9],

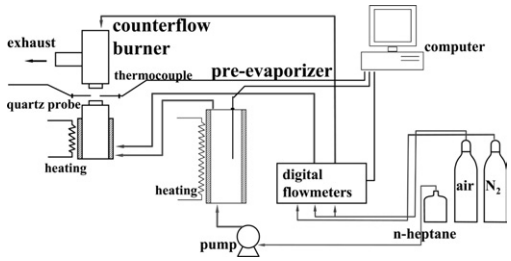

Fig. 1. Schematic diagram of the experimental apparatus.

$$a_g = \frac{2|V_O|}{L}\left(1 + \frac{|V_F|}{|V_O|}\sqrt{\frac{\rho_F}{\rho_O}}\right),$$

and to satisfy the momentum balance, $\rho_O V_O^2 = \rho_F V_F^2$.

The oxidizer was air at room temperature while the fuel stream consisted of mixtures of air and prevaporized *n*-heptane. The fuel nozzle was heated and the temperature was controlled to maintain the fuel-containing stream at a 400 K temperature at the burner exit. The air–*n*-heptane was mixed in a prevaporizer, which consisted of a stainless steel chamber that was electrically heated. The desired mass flowrate of *n*-heptane into the prevaporizer was maintained by a liquid pump, while gaseous nitrogen was introduced through the bottom of the chamber. Approximately, one-half of the chamber was filled with glass beads to increase the contact area between hot surface and liquid fuel, thereby enhancing the heat transfer, and to impede the flow, thereby increasing its residence time. The temperature of the fuel vapor–gaseous nitrogen mixture exiting the chamber was monitored by a thermocouple. Several flames were established for varying strain rates, equivalence ratios, and nitrogen dilutions. Three cases were more thoroughly analyzed, i.e., $a_g = 98.4$–$100.3\ s^{-1}$, $\phi = \infty$ (non-premixed); $a_g = 96.5$–$100.9\ s^{-1}$, $\phi = 3.7$–4.1; and $a_g = 97.7$–$99.3 + s^{-1}$, $\phi = 9.69$–10.93. (Here, the variations in the parameter values account for the experimental errors associated with the measurements). These cases will be addressed as $a_g = 100\ s^{-1}$, and $\phi = \infty$, 10, 4, respectively.

Temperature profiles of various flames were measured using a Pt–Pt 13% Rh thermocouple with a spherical bead diameter of 0.25 mm and wire diameter of 0.127 mm. The measured values were corrected for radiation heat losses from the bead, assuming a constant emissivity of 0.2 and a Nusselt number of 2.0 [1]. Species concentration

profiles were characterized using a Varian 3600CP Gas Chromatograph. Samples were drawn from the flame with a quartz microprobe that had a 0.95 mm tip diameter and 0.39 mm tip orifice. Constant vacuum was applied at the end of the line through a vacuum pump. The line carrying the sample to the GC was made of stainless steel and heated to prevent condensation. A portion of the sample was injected into a Hayesep DB 100/120 packed column connected to a thermal conductivity detector to measure light gases (up to C_2H_4) and another part into a Petrocol DH capillary column that was in line with a flame ionization detector to obtain the hydrocarbon distribution up to C_7H_{16}. Temperature programming was employed to minimize the analysis time. The temperature and pressure in the sampling loops were controlled to ensure that the same volume of gas was sampled for each analysis. The chromatogram peaks have been converted into mole fractions with calibration constants that were obtained separately for every species from known standards. Water molar fractions were evaluated through a mass balance of hydrogen atoms.

3. Reaction mechanism

The kinetic mechanism (SOX) used to model the flames was developed by extending a detailed oxidation scheme for several fuels [2,10]. Due to the hierarchical modularity of the mechanistic scheme, this model is based on a detailed submechanism of C_1–C_4 species. Assuming analogy rules for similar reactions, only a few fundamental kinetic parameters are required for the progressive extension of the scheme towards heavier species. The resulting kinetic model of hydrocarbon oxidation from methane up to *n*-octane consists of about 150 species and 3500 reactions.

We have selected this scheme for modeling since the subset of *n*-heptane oxidation reactions in the mechanism has been extensively tuned by validating experimental measurements for pure pyrolysis conditions, oxidation in a jet stirred and plug flow reactors, and on a large set of shock tube experiments [11]. The polycyclic aromatic hydrocarbons (PAHs), well-known for being soot precursors, are described in large detail in the scheme. The formation of the first aromatic rings by the C_2 and C_4 chemistry and by the resonantly stabilized radicals like propargyl and cyclopentadienyl (C_3H_3 and C_5H_5) has been carefully investigated [12,10]. Further growth of PAH species up to coronene ($C_{24}H_{12}$) is also modeled through the well-known hydrogen abstraction carbon addition (HACA) mechanism [13], which has been extensively validated for counterflow flames burning a variety of fuels [14]. The main consumption reactions of aromatics and PAHs are H abstraction reactions by H and OH radicals. The high temperature reactions have been validated against substantial experimental data [12,10].

Numerical simulations of counterflow flames were performed using the OPPDIF code [15] that is capable of modeling combustion between two opposed jets. The code was modified to handle the complex reaction mechanism and to account for thermal radiation through the optically thin model [16]. Most thermodynamic properties were obtained from Burcat and McBride [17] and unavailable properties were estimated using the group additivity and difference methods [18]. Transport properties were obtained from the CHEMKIN database [19], wherever available, while unavailable data were deduced through analogy with known species.

4. Results and discussion

Figure 2 presents the images of counterflow partially premixed flames established at strain rates $a_g = 50$ and 100 s^{-1} and fuel stream equivalence ratios $\phi = 4$, 6, 9, and 20. Fuel is introduced from the bottom nozzle. The double flame structure that is characterized by separate premixed and nonpremixed reaction zones becomes visually more distinct as a_g decreases and ϕ increases, which also increases the separation distance Δ between the two zones. The premixed reaction zone is established on the fuel-side of the stagnation plane at the location X_p where the local axial velocity V_x equals the burning velocity $S_{L,a}$ of the stretched flame. Since $S_{L,a}$ increases as ϕ is reduced, the premixed flame moves away from the stagnation plane toward the fuel nozzle to satisfy the condition $S_{L,a} = V_x$. The nonpremixed flame is established on the oxidizer side at the location X_n where the fuel and oxidizer fluxes meet in stoichiometric proportion. Therefore, the value of the reaction zone separation distance Δ increases as the fuel-side premixing approaches stoichiometric conditions. Increasing the strain rate has an opposite effect, since for larger flow velocities the location X_p is pushed toward the stagnation plane.

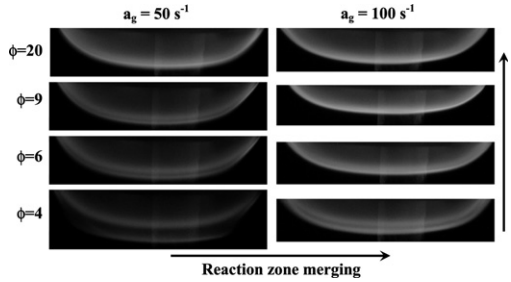

Fig. 2. Direct images of counterflow partially premixed flames established at $a_g = 50$ and 100 s^{-1} and fuel stream $\phi = 4$, 6, 9, and 20.

Soot is formed in the $\phi = 20$ and $a_g = 50\ s^{-1}$ flame for which the premixed reaction zone has a yellow–orange luminosity. This luminosity fades as ϕ is decreased, and is absent for the $a_g = 100\ s^{-1}$ flames.

The measured and simulated temperatures and axial velocity profiles are for three flames established at $a_g = 100\ s^{-1}$ and $\phi = 4$, 10, ∞ (i.e., for a nonpremixed flame) and are presented in Fig. 3. Since the momentum balance $\rho_O V_O^2 = \rho_F V_F^2$ is maintained for all three cases, the fuel and air nozzle velocities must be adjusted, although three flames have the same value of a_g. There is a small misalignment between the two measurements and simulations for all three cases regarding the peak temperatures. This has been partly attributed due to buoyancy effects that are not considered in the simulation [1]. The measured peak temperatures are higher than the corresponding simulated values, but the difference is within the ±50 K error in the thermocouple data. The evolution from a single nonpremixed reaction zone to a double flame structure is evident upon comparing the temperature and velocity profiles for the three cases. The temperature profiles become spatially broader as the value of ϕ decreases. For $\phi = 4$, the velocity profile clearly exhibits the gas expansion caused by the fuel side premixed reaction zone.

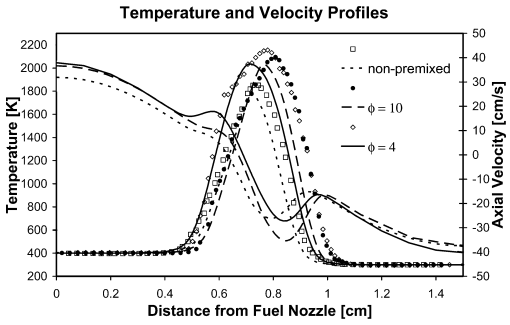

Fig. 3. Measured and simulated temperature profiles and simulated velocity profiles for three flames established at $a_g = 100\ s^{-1}$ and $\phi = 4$, 10, and ∞ (nonpremixed flame).

Table 1 compares our measurements of the peak temperatures and specific major and minor species mole fractions with those for *n*-heptane flames found in the literature [1,6]. The major species are the major products (CO_2 and H_2O) and intermediates (CO and H_2), and C_2H_2 and C_2H_4 are chosen since they lie along the C_2 decomposition pathway that leads to soot precursors. The first comparison pertains to our measurements of a nonpremixed flame with the results from [1]. Our measured peak temperature is higher by 100 K, which is attributed to the lower a_g value in our experiment (100 versus 150 s^{-1} in [1]). Nonetheless, the peak concentrations of CO, H_2, H_2O, and summed C_2 species are in very good agreement, but there is a discrepancy in the CO_2 measurements. The nonpremixed flame reported in [6] was enriched with oxygen in order to match the peak temperature of their $\phi = 2.8$ partially premixed flame. In addition, liquid *n*-heptane was introduced in the form of a spray. Therefore, it is difficult to make a direct comparison of the strain rate for that flame and our measurements. That flame contains larger concentrations of oxidation products. Our measurements of the peak amounts of C_2 species differ from theirs, but the summed values of the respective C_2 compounds are virtually identical. There is a general agreement between various facets of our nonpremixed flame measurements and the results of [1,6]. This provides some consistency to the three sets of data.

Our investigation shows that the peak flame temperature increases with increasing premixing of the fuel stream. The peak temperature of the $\phi = 2.8$ flame in [6] is lower than our measurement in a $\phi = 4$ flame. Apart from measurement uncertainties and different fluid dynamic conditions at the boundaries [20], it is possible that the $\phi = 2.8$ flame was established at a higher a_g value. The peak temperatures of all partially premixed cases are ~2100 K, which are lower than the adiabatic flame temperature of 2274 K. All three measurements show that the value of Δ increases as ϕ decreases, i.e., with greater partial

Table 1
Comparison of experimental *n*-heptane counterflow flames at various values of a_g (s^{-1}) and ϕ

	a_g	ϕ	$N_{2,F}$	$O_{2,O}$	Δ	T	CO	CO_2	H_2	H_2O	C_2H_2	C_2H_4
Present	100	∞	0.88	0.21	—	1850	0.034	0.056	0.011	0.104	0.011	0.012
[1]	150	∞	0.85	0.21	—	1750	0.033	0.07	0.014	0.11	0.025	−Sum
[6]	Spray	∞	0.844	0.47	—	2100	0.065	0.105			0.005	0.02
Present	100	10		0.21	1	2100	0.074	0.107	0.043	0.146	0.021	0.033
Present	100	4		0.21	1.6	2150	0.089	0.109	0.037	0.159	0.018	0.03
[6]	Spray	2.8		0.21	2.5	2050	0.09	0.1			0.008	0.025

Temperatures are in *K*, peak concentrations are in molar fractions, and flame spacing Δ is in mm. The subscripts F and O refer to the respective concentrations at the fuel and oxidizer nozzle. Similar conditions are highlighted.

premixing. The peak CO_2 and H_2O concentrations are relatively insensitive to partial premixing. The CO peak is on the premixed side and it increases as larger amounts of oxygen are supplied by decreasing the fuel-side equivalence ratio. Likewise, the increasing amount of fuel-side oxygen reduces the peak H_2 concentration upstream of the premixed fraction zone. Not surprisingly, the increased oxidation with decreasing ϕ also reduces the peak concentrations of the C_2 species. This shows the influence of partial premixing on the formation of C_2 related soot precursors. It is known that partially premixed flames are less sooting than their nonpremixed or premixed counterparts [21,22].

Figures 4A–L present the structures of two *n*-heptane/air partially premixed flames with a high ($\phi = 4$) and low ($\phi = 10$) level of fuel–air premixing. The temperature data from Fig. 3 are repeated, but also contain the uncorrected temperatures, which are useful, since the modeling community sometimes applies its own adjustments. The double flame structure is clear by observing the measured temperatures in Figs. 4A and B, but not so through the simulations. The visually observed locations of the premixed and nonpremixed reaction zones are marked in the figures. The measured and simulated temperatures and major species concentration profiles are in relatively good agreement. However, the comparison for benzene is not as good, but both the simulations and experiments show that the peak benzene mole fraction decreases with increasing partial premixing. The good agreement between the predicted and experimental nitrogen concentration profiles for both flames shows that transport phenomena are well modeled in the simulations.

There is a discrepancy in the oxidizer profiles in the vicinity of the two reaction zones in Fig. 4C and in the nonpremixed zone in Fig. 4D. While the simulations are able to qualitatively predict the measured oxygen concentrations, it appears that the overall oxidation in the model is slower (which leads to the lower predicted peak

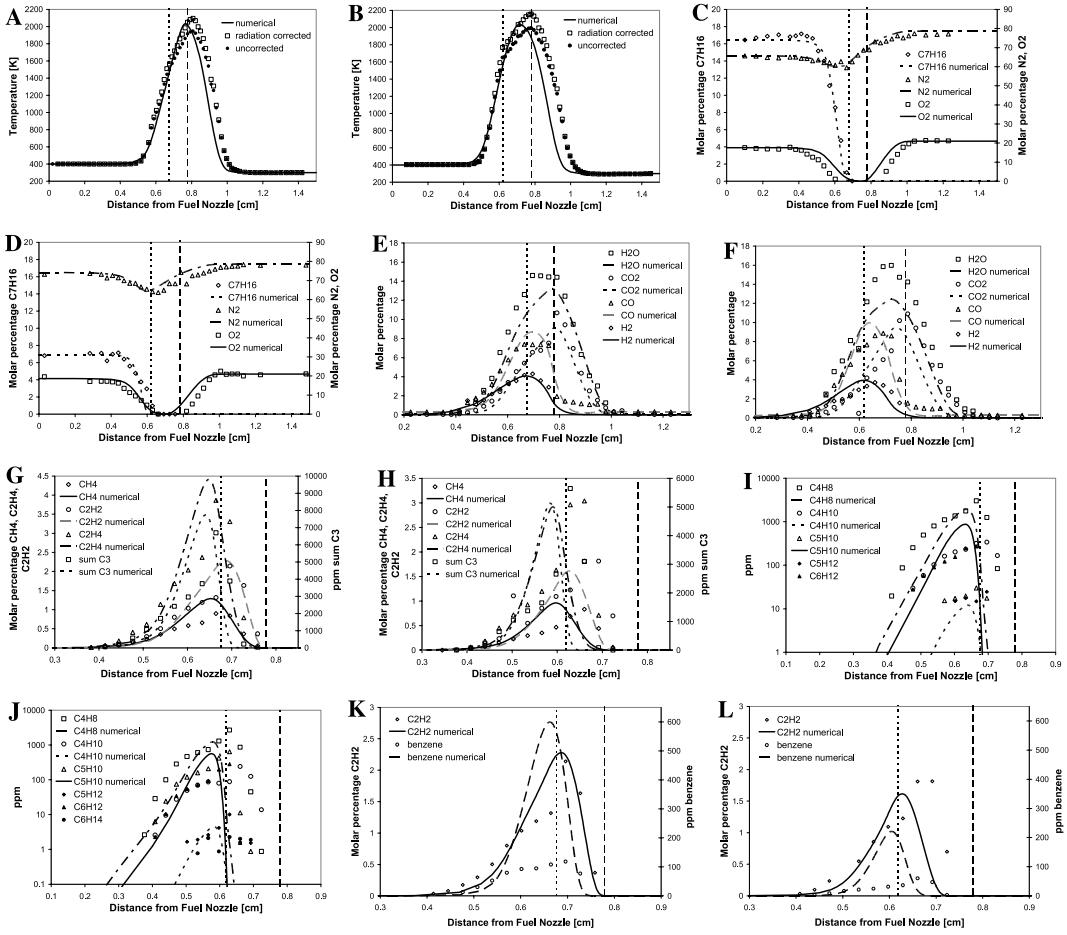

Fig. 4. Measured and simulated temperature and species concentration profiles (as marked) for two flames established at $a_g = 100\ s^{-1}$ and $\phi = 4$ (left) and 10 (right), respectively.

concentrations of CO_2 and H_2O). However, the fuel consumption is appropriately modeled. The premixed reaction zone (on the left in the figures) propagates upstream. It burns in the fuel-rich mixture and produces intermediate species such as CO and H_2. These species are transported to the nonpremixed reaction zone where they burn to produce CO_2 and H_2O. In a purely nonpremixed flame the CO formation is immediately followed by oxidation on the air-side of the flame. The carbon monoxide and carbon dioxide peaks are spatially closer in nonpremixed flames than those for partially premixed flames. The separation between these peaks increases as the equivalence ratio is lowered, and the flame transitions to two distinct, premixed and nonpremixed, interacting structures.

Figures 4G and H present the concentration profiles of light hydrocarbon species. The agreement between simulated and predicted profiles is good. For both flames the C_2 species have peaks in the premixed reaction zone, implying that the C_2-decomposition occurs there. These intermediate species are consumed before reaching the nonpremixed reaction zone. The peak concentrations of the species occur in the order $CH_4 > C_2H_2 > C_2H_4 >$ sum of all C_3 species. The peak values of these species decrease with the increasing oxidizer availability as the equivalence ratio is lowered.

The profiles of C_4, C_5, and C_6 paraffins and olefins are presented in Figs. 4I and J. The predicted values of these species do not agree with the measurements, with some peak values differing by more than one order of magnitude. However, due to their small concentrations, it appears that their effect on the overall reaction path is marginal. These species peaks occur immediately upstream of the premixed flame and are rapidly consumed thereafter. The concentrations of olefins are ten times larger than those of the corresponding paraffins, confirming that hydrogen abstraction reactions are important in the premixed reaction zone. The model does not include some measured species, such as C_5H_{12} (peak value of 4.2 ppm for $\phi = 4$), C_6H_{12} (281 ppm), and C_6H_{14} (2.3 ppm), but these occur in small concentrations.

Figures 4K and L can also provide some insight into the soot formation pathway for *n*-heptane–air partially premixed flames. Acetylene and benzene are considered to be soot precursors. In the $\phi = 4$ flame the acetylene peak concentration is three times lower than in the $\phi = 10$ partially premixed flame. The benzene peak concentration is likewise approximately halved. The oxidizer contained in the premixed fuel stream drives the reactions towards oxidation rather than pyrolysis. The oxidizer is present in partially premixed flames throughout the combustion system and there are no regions characterized by simultaneous high temperature and high fuel concentration. As a result pyrolysis reactions leading to soot formation are greatly diminished.

5. Conclusions

Experiments were performed to characterize the structure of *n*-heptane–air nonpremixed and partially premixed counterflow flames by varying the fuel stream equivalence ratio. A detailed comparison between measurements and simulations is provided for high and low premixing cases for the profiles of temperature and concentrations of N_2, O_2, C_7H_{16}, CO, CO_2, H_2, CH_4, C_2H_2, C_2H_4, C_3 hydrocarbons, C_4H_8, C_4H_{10}, C_5H_{10}, C_5H_{12}, C_6H_{12}, C_6H_{14}, and C_6H_6. The measurements were compared with the experimental results reported in the literature and there is agreement regarding major facets of these data.

As the equivalence ratio is increased, the spatial separation between the rich premixed and nonpremixed reaction zones increases, and the peak temperature, which occurs in the nonpremixed zone, slightly increases. There is a simultaneous evolution from a single nonpremixed reaction zone to a double flame structure. The fundamental structure of a partially premixed flame is as follows. The premixed reaction zone propagates upstream where it burns in the fuel-rich mixture and produces intermediate species such as CO and H_2. These are transported to the nonpremixed reaction zone where they oxidize to produce CO_2 and H_2O. The oxidizer is present in partially premixed flames throughout the combustion system and there are no regions characterized by simultaneous high temperature and high fuel concentration. As a result pyrolysis reactions leading to soot formation are greatly diminished. The concentrations of olefins are ten times larger than those of the corresponding paraffins, confirming that hydrogen abstraction reactions are important in the premixed reaction zone.

Acknowledgments

This research was supported by the National Science Foundation Combustion and Plasma Systems Program for which Dr. Farley Fisher is the Program Director, and by the NASA Microgravity Research Division for which Dr. Uday Hegde serves as the technical monitor.

References

[1] R. Seiser, L. Truett, D. Trees, K. Seshadri, *Proc. Combust. Inst.* 27 (1998) 649–657.
[2] P. Berta, A. Mukhopadhyay, I.K. Puri, S. Granata, T. Faravelli, E. Ranzi, in: *Proceedings of the 24th event of the Italian Section of the Combustion*

Institute, V-3, 2001. Available from: <http://ppf.me.uic.edu/~ikpuri/papers.htm>.
[3] Z. Shu, B.J. Krass, C.W. Choi, S.K. Aggarwal, V.R. Katta, I.K. Puri, *Proc. Combust. Inst.* 27 (1998) 625–632.
[4] S.C. Li, F.A. Williams, *Combust. Flame* 118 (1999) 399–414.
[5] R. Azzoni, S. Ratti, I.K. Puri, S.K. Aggarwal, *Phys. Fluids* 11 (1999) 3449–3464.
[6] S.C. Li, F.A. Williams, *Proc. Combust. Inst.* 28 (2000) 1031–1038.
[7] H.S. Xue, S.K. Aggarwal, *AIAA J.* 39 (2001) 637–648.
[8] H.S. Xue, S.K. Aggarwal, *Combust. Flame* 132 (2003) 723–741.
[9] I.K. Puri, K. Seshadri, *Combust. Flame* 65 (1986) 137–150.
[10] A. Goldaniga, T. Faravelli, E. Ranzi, *Combust. Flame* 122 (2000) 350–358.
[11] E. Ranzi, P. Gaffuri, T. Faravelli, P. Dagaut, *Combust. Flame* 103 (1995) 91–106.
[12] T. Faravelli, A. Goldaniga, E. Ranzi, *Proc. Combust. Inst.* 27 (1998) 1489–1495.
[13] H. Wang, M. Frenklach, *Combust. Flame* 110 (1997) 173.
[14] F. Xu, A.M. El-Leathy, C.H. Kim, G.M. Faeth, *Combust. Flame* 132 (2003) 43–57.
[15] A.E. Lutz, R.J. Kee, J.F. Grcar, F.M. Rupley, Report No. SAND96-8243, Sandia National Laboratories, 1997.
[16] B. Pogliani, M. Bundy, A. Hamins, I.K. Puri, in: *Proceedings of the 2nd Joint Technical Meeting of the US Sections of The Combustion Institute*, Paper No. 218, Oakland, CA, March 25–28, 2001.
[17] A. Burcat, B. McBride, 1997 *Ideal Gas Thermodynamic Data for Combustion and Air-Pollution Use*, Report No. TAE 804 Technion Israel Institute of Technology, Aerospace Engineering, 1997.
[18] S.W. Benson, *Thermochemical Kinetics*, second ed., John Wiley, New York, 1976.
[19] R.J. Kee, G. Dixon-Lewis, J. Warnatz, M.E. Coltrin, J.A. Miller, *The Chemkin Transport Data Base*, Report No. Sandia National Laboratories, 1986.
[20] H.K. Chelliah, C.K. Law, T. Ueda, M.D. Smooke, F.A. Williams, *Proc. Combust. Inst.* 23 (1990) 503–511.
[21] H.S. Hura, I. Glassman, *Proc. Combust. Inst.* 22 (1988) 371–378.
[22] M. Choinski, C. Arana, S. Sen, I.K. Puri, *Proceedings of the 3rd Joint Technical Meeting of the US Sections of The Combustion Institute*, Paper No. F10, Chicago, IL, March 16–19, 2003.

Comments

Xiao Qin, Princeton University, USA. It seems impractical to use your detailed chemistry in an engineering situation. Have you tried to obtain a reduced mechanism that can give you similar predictions?

Reply. We have investigated the structure of partially premixed flames burning *n*-heptane in air using a detailed mechanism that consists of a number of elementary steps. The mechanism better represents the real combustion chemistry than a reduced mechanism. The development of a reduced mechanism is an entirely separate topic and was not the focus of our investigation. The use of relatively large chemical mechanisms to investigate flame structure is by now routine and unquestioned.

●

R.P. Lindstedt, Imperial College, UK. The discrepancy for benzene is large. Could you please outline the major formation channels in your current mechanism and comment on experimental uncertainties (error bars) in your measurements?

Reply. Benzene formation pathways in the reaction mechanism include those for C_2 and C_4 chemistry [12 in the paper], C_3H_3 and C_5H_5 radical recombination [10 in the paper], and the HACA mechanism [13, 14 in the paper]. A reaction pathway analysis was not performed, in large part since tuning of the mechanism was not an objective. Previous work [10–13 in the paper] should provide greater insight into benzene formation and consumption in this scheme. Our species concentration measurements have $\pm 5\%$ uncertainty. Similar previous investigations [1, 6 in the paper] that we used for comparison did not, unfortunately, include benzene measurements and ours appear to be the first literature entry in this regard.